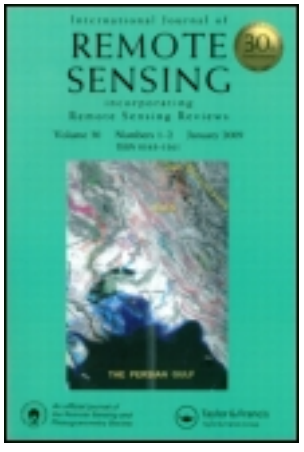

International Journal of Remote Sensing

Publication details, including instructions for authors and subscription information:
http://www.tandfonline.com/loi/tres20

Estimation of the dynamics and yields of cereals in a semi-arid area using remote sensing and the SAFY growth model

Aicha Chahbi[ab], Mehrez Zribi[a], Zohra Lili-Chabaane[b], Benoit Duchemin[a], Marouen Shabou[ab], Bernard Mougenot[a] & Gilles Boulet[a]

[a] CESBIO (CNRS/UPS/IRD/CNES), Toulouse, France

[b] INAT-LRSTE (Carthage University), 43, Avenue Charles Nicolle 1082, Tunis, Tunisia

Published online: 13 Feb 2014.

To cite this article: Aicha Chahbi, Mehrez Zribi, Zohra Lili-Chabaane, Benoit Duchemin, Marouen Shabou, Bernard Mougenot & Gilles Boulet (2014) Estimation of the dynamics and yields of cereals in a semi-arid area using remote sensing and the SAFY growth model, International Journal of Remote Sensing, 35:3, 1004-1028, DOI: 10.1080/01431161.2013.875629

To link to this article: http://dx.doi.org/10.1080/01431161.2013.875629

International Journal of Remote Sensing, 2014
Vol. 35, No. 3, 1004–1028, http://dx.doi.org/10.1080/01431161.2013.875629

Taylor & Francis
Taylor & Francis Group

Estimation of the dynamics and yields of cereals in a semi-arid area using remote sensing and the SAFY growth model

Aicha Chahbi[a,b], Mehrez Zribi[a]*, Zohra Lili-Chabaane[b], Benoit Duchemin[a], Marouen Shabou[a,b], Bernard Mougenot[a], and Gilles Boulet[a]

[a]*CESBIO (CNRS/UPS/IRD/CNES), Toulouse, France;* [b]*INAT-LRSTE (Carthage University), 43, Avenue Charles Nicolle 1082, Tunis, Tunisia*

(*Received 28 January 2013; accepted 30 November 2013*)

In semi-arid areas, a strongly variable climate represents a major risk for food safety. An operational grain yield forecasting system, which could help decision-makers to make early assessments and plan annual imports, is thus needed. It can be challenging to monitor the crop canopy and production capacity of plants, especially cereals. In this context, the aim of the present study is to analyse the characteristics of two types of irrigated and non-irrigated cereals: barley and wheat. Through the use of a rich database, acquired over a period of two years for more than 30 test fields, and from 20 optical satellite SPOT/HRV images, two research approaches are considered. First, statistical analysis is used to characterize the vegetation's dynamics and grain yield, based on remotely sensed (satellite) normalized difference vegetation index (NDVI) measurements. A relationship is established between the NDVI and LAI (leaf area index). Different robust relationships (exponential or linear) are established between the satellite NDVI index acquired from SPOT/HRV images, just before the time of maximum growth (April), and grain and straw, for barley and wheat vegetation covers. Following validation of the proposed empirical approaches, yield maps are produced for the studied site. The second approach is based on the application of a Simple Algorithm for Yield Estimation (SAFY) growth model, developed to simulate the dynamics of the LAI and the grain yield. An inter-comparison between ground yield measurements and SAFY model simulations reveals that yields are underestimated by this model. Finally, the combination of multi-temporal satellite measurements with the SAFY model estimations is also proposed for the purposes of yield mapping. Although the results produced by the SAFY model are found to be reasonably well correlated with those determined by satellite measurements (NDVI), the grain yields are nevertheless underestimated.

1. Introduction

The world's population has been constantly increasing over the last half century. This growth has been accompanied by an increase in the consumption of agricultural products, especially cereals, such that it is becoming increasingly important for scientists and decision-makers to be able to estimate grain yields at regional and national levels. An operational grain-yield forecasting system is thus required, and could help decision-makers to make timely decisions and plan annual imports (Justice and Becker-Reshef 2007). Many models, based on the use of remote sensing or agro-meteorological models, have been developed to estimate the biomass and grain yield of cereals (Barnett and

*Corresponding author. Email: mehrez.zribi@cesbio.cnes.fr

Thompson 1982; Benedetti and Rossinni 1993; Moriondo, Maselli, and Bindi 2007; Balaghi et al. 2008; Becker-Reshef et al. 2010; Laurila et al. 2010).

Remote sensing has demonstrated its strong potential for the monitoring of dynamics and temporal variations of soil and vegetation, mainly because it provides wide spatial coverage and has consistent internal data sets (Zribi, André, and Decharme 2008; Amri et al. 2011). Optical remote sensing has demonstrated its strong potential for the monitoring of vegetation dynamics and temporal variations, mainly because it provides wide spatial coverage and has consistent internal data sets. In particular, the normalized difference vegetation index (NDVI) expresses the contrast in reflectance between the red and near-infrared regions of a surface spectrum (Rouse et al. 1974). The NDVI is simple to calculate, can be related to green vegetation cover or vegetation abundance, and is expressed by: NDVI = (NIR − RED)/(NIR + RED), where NIR is the near-infrared reflectance and RED is the reflectance at red wavelengths. The NDVI is sensitive to the presence of green vegetation (Sellers 1985) and has been used for several regional and global applications, in studies concerning the distribution and potential photosynthetic activity of vegetation (Deblonde and Cihlar 1993; Propastin and Kappas 2009). Efforts have been made to develop various models and approaches for the purposes of forecasting the yields of different crops in different regions throughout the globe. Most studies related to the estimation of cereal yields make use of low resolution sensors (Bastiaanssen and Ali 2003; Balaghi et al. 2008; Kogan et al. 2013). Balaghi et al. (2008) proposed the use of empirical ordinary least squares regression models to forecast yields at provincial and national levels. Their predictions were based on decadal NDVI/AVHRR data, decadal accumulated rainfall, and average monthly air temperatures. Becker-Becker-Reshef et al. (2010) combined a new BRDF-corrected daily surface reflectance data set, developed from NASA's Moderate Resolution Imaging Spectroradiometer (MODIS), with detailed official crop statistics. They used these combined data to develop an empirical, generalized approach to the forecasting of wheat yields. This was based on a single, generalized model, which was applied at the level of the state of Kansas (USA) and has been shown to be directly applicable to Ukraine. Yield estimations are also relevant to other types of vegetation, including rice (Wang et al. 2010; Wei-guo, Hua, and Li-Hua 2011), soybean and soya (Prasad et al. 2006), olives (Maselli et al. 2012), citrus fruit (Ye et al. 2006), and maize and sunflower crops (Claverie et al. 2012).

In recent decades, there has also been a growing interest in approaches based on agro-ecological process models combined with remote sensing. Vegetation models based on climatic and agronomic data have demonstrated a good degree of correlation between estimated and measured variables at the local level (Bastiaanssen and Ali 2003; Duchemin et al. 2008). These models simulate key variables, including the leaf area index (LAI). The model proposed by Bastiaanssen and Ali (2003) combines the photosynthetically active radiation (PAR) model of Monteith (1972), the light-use efficiency model of Field, Randerson, and Malmstrom (1995), and the surface energy balance model of Bastiaanssen et al. (1998) to estimate the growth of irrigated crops. To forecast crop yields, these authors used the National Oceanic and Atmospheric Administration's (NOAA) Advanced Very High Resolution Radiometer (AVHRR; http://noaasis.noaa.gov/NOAASIS/ml/avhrr.html) instrument during periods of crop irrigation. Most of these studies have been carried out in Europe or North America, where generally high levels of cereal production are encountered.

Lobell et al. (2003) estimated crop yields using AVHRR imagery over northwest Mexico. Remotely sensed estimations of the fraction of absorbed photosynthetically active radiation (fAPAR) were incorporated into a simple model based on crop light-use efficiency estimations derived from Monteith (1972, 1977), to predict wheat yields and optimal planting dates.

The aim of the present study is to evaluate the feasibility of three approaches: high-resolution remote-sensing imagery, the agro-meteorological SAFY (Simple Algorithm for Yield Estimation) model, and combined use of the SAFY model with remotely sensed data, to estimate the dynamics and yields of cereals in the context of semi-arid, low-productivity regions in North Africa.

Section 2 describes the study site and the experimental satellite and ground measurement database. Section 3 is dedicated to the statistical analysis of this data, used to estimate the dynamics and yields of cereals derived from the remotely sensed NDVI. In Section 4, the use of the SAFY model for the estimation of vegetation cycle dynamics and yields is described. Then, the combined use of the SAFY model and remotely sensed data is presented. Our conclusions are given in section 5.

2. Experimental database

2.1. Study area

The Kairouan plain (Zribi et al. 2011) is situated in central Tunisia (9° 30′ E, 10° 15′ E, 35° N, 35° 45′ N) (Figure 1). The climate in this region is semi-arid, with an average annual rainfall of approximately 300 mm, characterized by a rainy season lasting from October to May, with the two rainiest months being October and March. As is generally the case in semi-arid areas, the rainfall patterns in this area are highly variable in time and space. The mean temperature in Kairouan City is 19.2°C (minimum 10.7°C in January and maximum 28.6°C in August) and the mean annual potential evapotranspiration (Penman) is close to 1600 mm. The landscape is mainly flat and the vegetation in this area is dominated by agriculture (cereals, olive trees, and market gardens). There are various types of crop, and their rotation is typical of semi-arid regions. The aquifer of the Kairouan plain represents the largest basin in central Tunisia. It is fed by the infiltration of surface waters during floods in the natural regime, or at the time of dam releases since the

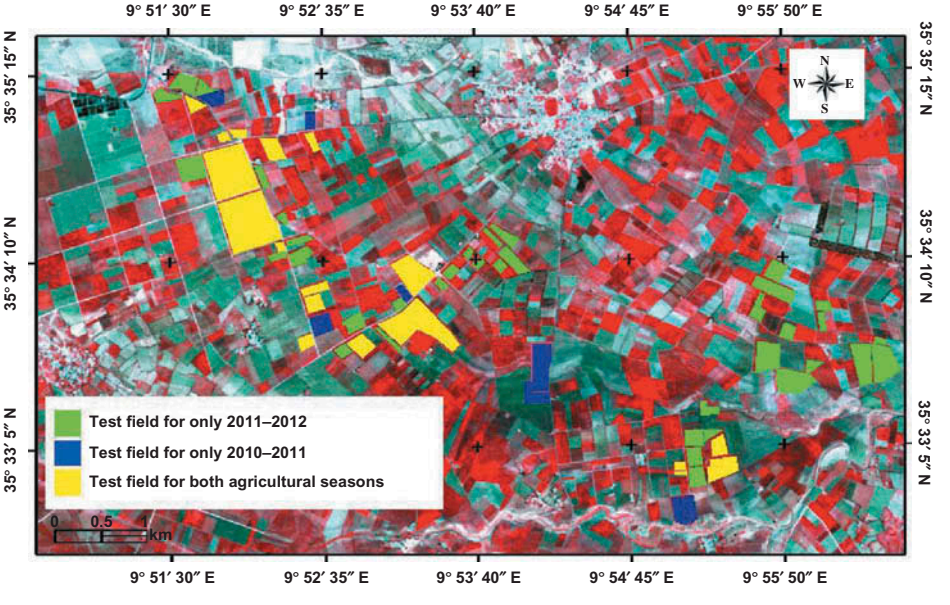

Figure 1. Illustration of the study site.

Table 1. Satellite acquisition dates.

Image	Acquisition date	Sensor
1	24 December 2010	SPOT5
2	29 January 2011	SPOT5
3	19 February 2011	SPOT5
4	17 March 2011	SPOT5
5	5 April 2011	SPOT4
6	28 April 2011	SPOT5
7	18 May 2011	SPOT5
8	3 July 2011	SPOT5
9	6 November 2011	SPOT5
10	13 January 2012	SPOT5
11	28 February 2012	SPOT5
12	31 March 2012	SPOT5
13	4 May 2012	SPOT4
14	25 May 2012	SPOT4
15	6 July 2012	SPOT4

construction of the Sidi Saad and El Haouareb dams. Surface and groundwater streams drain into the Sebkha Kelbia, a large salt lake.

2.2. *Satellite data*

For the purposes of monitoring surface parameters and gaining an understanding of the vegetation dynamics on the Kairouan plain, 15 images acquired by the SPOT 5 satellite were analysed (Table 1). These images were acquired with a repeat time of approximately 21 days and high spatial resolution, equal to 10 m. All of the acquired images were orthorectified using the ground control point technique. The resulting mismatch between these images and the reference image was less than ± 0.5 pixel. In a second step, the orthorectified images were calibrated to derive the TOA (top of atmosphere) reflectances, and then atmospherically corrected to obtain the TOC (top of canopy) reflectances. The raw digital values were initially converted to TOA reflectances using the same absolute calibration techniques as those operationally applied to SPOT image data (Meygret 2005). The atmospheric correction needed to determine the TOC reflectances relies on inversion of the 6S radiative transfer model (Rahman and Dedieu 1994; Berthelot and Dedieu 1997), based on the use of look-up tables. This model requires input parameters such as the aerosol optical thickness (AOT) at 550 nm, size distribution and refractive index of the aerosols, water vapour content, ozone content, and atmospheric pressure. The water vapour content was determined from measurements recorded at the study site, the ozone content was obtained from ozone monitoring instrument (OMI) data (available at http://toms/gsfc.nasa.gov), and the surface atmospheric pressure was retrieved from http://www.tutiempo.net.

2.3. *Ground measurements*

Simultaneous to the satellite data acquisitions, ground campaigns were carried out approximately once every two weeks on a large number of test plots, during two agricultural seasons (2010–2011 and 2011–2012). During the first year a total of 27 test fields, including 18 irrigated and 9 non-irrigated cereal fields, were used for the ground truth measurements (Figure 1), whereas during the second season, 55 test fields, including

Table 2. Number and type of test fields for the two agricultural seasons.

Agricultural year	Number and type of fields
2010/2011	Non-irrigated wheat: 6 Irrigated wheat: 14 Non-irrigated barley: 3 Irrigated barley: 4
2011/2012	Non-irrigated wheat: 13 Irrigated wheat : 27 Non-irrigated barley: 6 Irrigated barley: 9

36 irrigated and 19 non-irrigated cereal fields, were analysed. Two types of cereal were considered: wheat and barley in the case of the selected test fields. Table 2 provides a detailed breakdown of the characteristics of these fields.

The *in situ* measurements involved mainly water content, height, LAI of the vegetation, and cereal yields.

2.3.1. *Leaf Area Index*

LAI is defined as the total one-sided area of leaf tissue per unit of ground surface area. According to this definition, LAI is a dimensionless quantity characterizing the canopy of an ecosystem. Two different approaches can be used to estimate LAI: directly through destructive sampling, or indirectly by applying methods based on ground-level gap fraction measurements. In the present study, an indirect method is used, in which LAI is derived from hemispherical digital photography. A binary classification of green elements and soil is proposed, in order to compute the gap fraction at a 57.5° zenith angle, from which an estimation of LAI is then derived (Kirk et al. 2009; Baret et al. 2010; Sandmann, Graefe, and Feller 2013).

These measurements were applied to each cereal field, on different days during the vegetation season. Thirty LAI estimations were made for each field, within two 20 m × 20 m square areas. The LAI measurements were made during the same week as that during which the SPOT 5 satellite images were recorded, in order to limit any discrepancies between ground and satellite measurements.

Figure 2(*a*) plots the variations in these measured quantities for three test fields, two of which were irrigated. The third field was rainfed during the second season. First, a LAI maximum, which occurred after a period of accelerated growth, can be observed during the first two weeks of April. Secondly, a clear difference can be seen between the irrigated and rainfed vegetation cycles, with a greater increase in the LAI parameter at the beginning of the vegetation cycle in the case of the irrigated fields.

2.3.2. *Cereal yield*

For each test field, ten sample measurements were taken along the two field diagonals, using a 75 cm × 75 cm frame. The cereal yields were then measured: the number of stalks, the weight of the grain, and the weight of the straw were recorded. The yields and quantities of grain lost during harvesting were studied simultaneously. As a result of the use of data taken from both rainfed and irrigated fields, the estimated yields have a large dynamic range, between 1300 kg ha^{-1} and 10,300 kg ha^{-1}, with a mean value of 4300 kg ha^{-1} for wheat, and between 1500 kg ha^{-1} and 5500 kg ha^{-1}, with a mean value of 3400 kg ha^{-1}, for

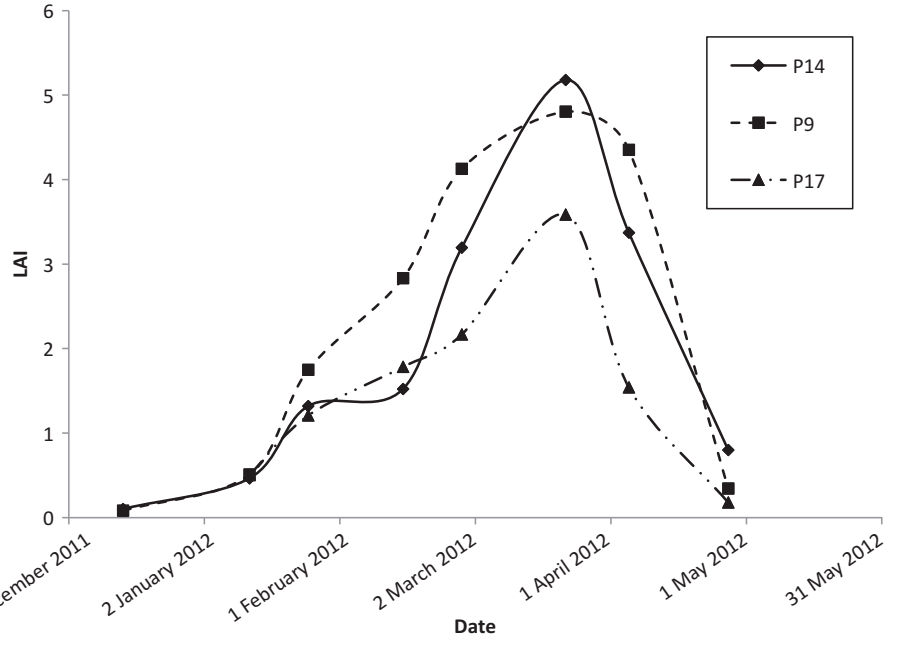

Figure 2. (*a*) Illustration of the evolution of LAI measurements for three test fields: irrigated (P14 and P9) and rainfed (P17) fields, during the 2011–2012 agricultural season. (*b*) Comparisons between the error bars of measured grain yield and NDVI extracted from satellite images for barley (*a*) and wheat (*b*).

barley. Figure 2*(b)* shows the error bars corresponding to the measured grain yield and NDVI extracted from satellite images at the beginning of April, for the 82 test fields. The mean standard deviation of NDVI is 0.067, with an average value for all test fields equal to 0.58. For the measured grain yields, the average value for all fields is equal to 3400 kg ha^{-1}, and the mean standard deviation for all test fields is equal to 970 kg ha^{-1}.

2.4. Land-use mapping

Land-use identification (Figure 3) is an essential step in the mapping of yields over all cereal fields. For this, land-use mapping was implemented, based on a decision tree and using two types of satellite data: four SPOT images acquired at four different times of the year were used to identify different vegetation (Table 3) cycles, and SRTM data were used for relief identification. A decision tree classification approach was used, from which 11 classes of land use were identified: pluvial olive trees, irrigated olive trees, irrigated winter vegetables, irrigated summer vegetables, bare soils, cereals, urban areas, mountainous areas, wadi beds, dams, and coastal salt flats ('sebkhas'). For all of these classes, thresholds were considered for one or two images. Test fields were used during the learning phase in order to identify empirical NDVI thresholds allowing the different classes to be distinguished. For example, for summer vegetables, an empirical NDVI threshold was applied to the image acquired in July (NDVI > 0.3). In the case of winter vegetables, the image acquired at the end of autumn or the beginning of summer was used. During these periods of the year, vegetables have the highest NDVI index. For the cereal classes (irrigated or non-irrigated, wheat or barley), the satellite data acquired in March or April, corresponding to the cereals' maximum growth, were used. The digital terrain

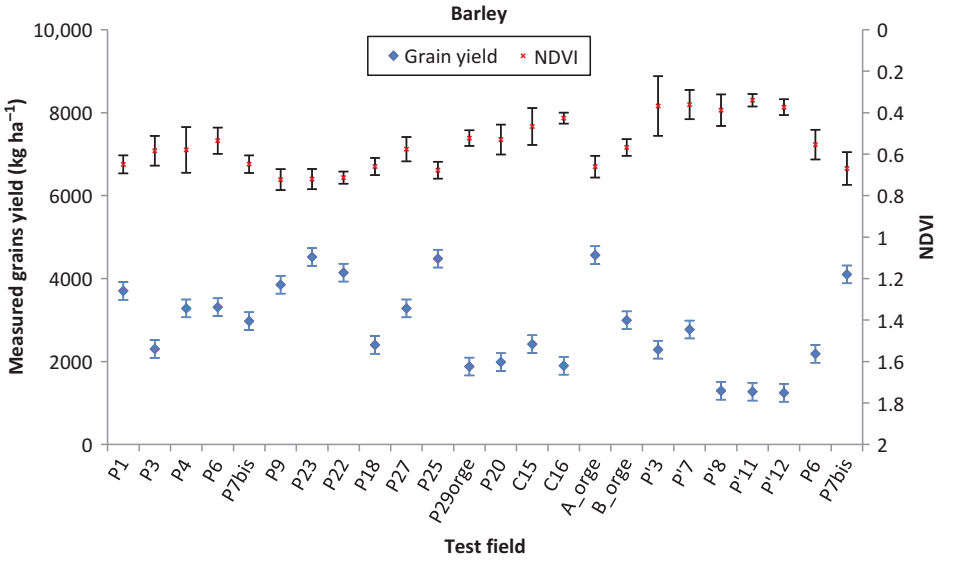

(*a*)

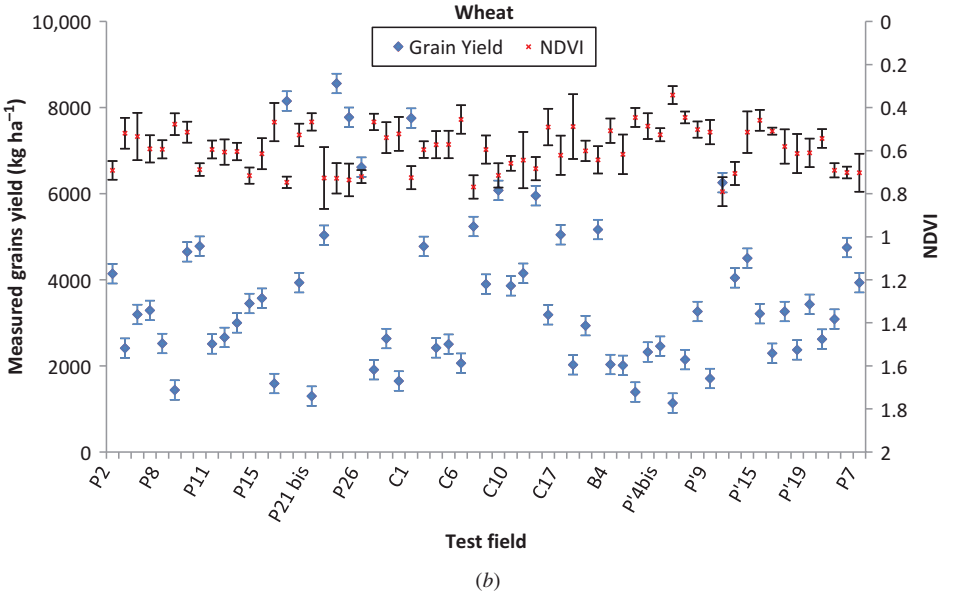

(*b*)

Figure 2. (*Continued*).

model (DTM) provided by the Shuttle Radar Topography Mission (SRTM, http://srtm.usgs.gov/) allowed high-relief areas to be eliminated from the land-use analysis. In order to validate these remotely sensed classifications, a confusion matrix was produced by comparing the classification results obtained from more than 100 test fields, characterized by different types of land use. This analysis revealed an overall accuracy of approximately 80%, and greater than 90% in the case of cereals. The non-irrigated olive tree class covers 43% of the studied site, whereas the wheat class corresponds to 12% of the surface area of the study site.

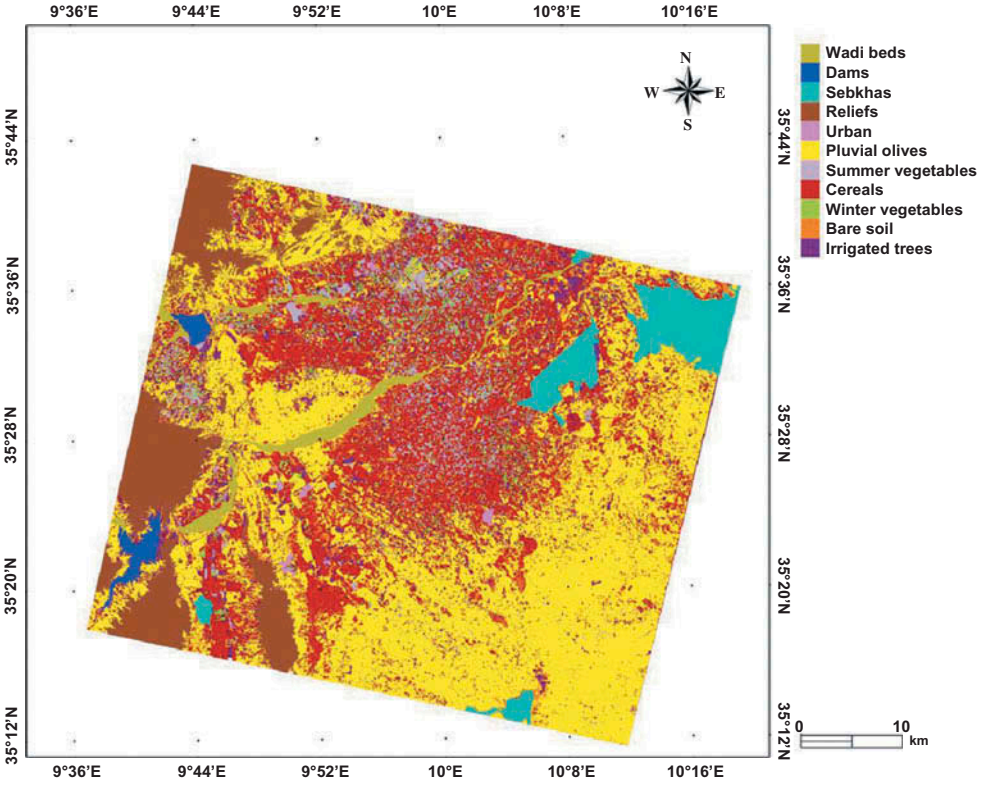

Figure 3. Land-use map for the 2011–2012 agricultural season.

Table 3. Satellite imagery used to produce the land-use map.

Agricultural year	Spot 5 satellite imagery
2010/2011	24 December 2010, 29 January 2011, 17 March 2011, 28 April 2011 and 3 July 2011
2011/2012	6 January 2011, 13 January 2012, 31 March 2012 and 6 July 2012

Once established, the land-use map can be used to extract a cereal mask for the two agricultural seasons under study.

3. Statistical analysis of the relationship between cereal yields and satellite observations

The aim of this section is to evaluate the potential of remote sensing, combined with statistical analysis, for the estimation of barley and wheat yields.

3.1. Relationship between SPOT–NDVI and cereal yields

Figure 4 illustrates the relationship between NDVI acquired on 17 March 2011 and 31 March 2012, and the grain and straw yield measurements (Y_{grain} and Y_{straw}) obtained at the end of the cereal season. For the first data set, including 44 fields and covering a

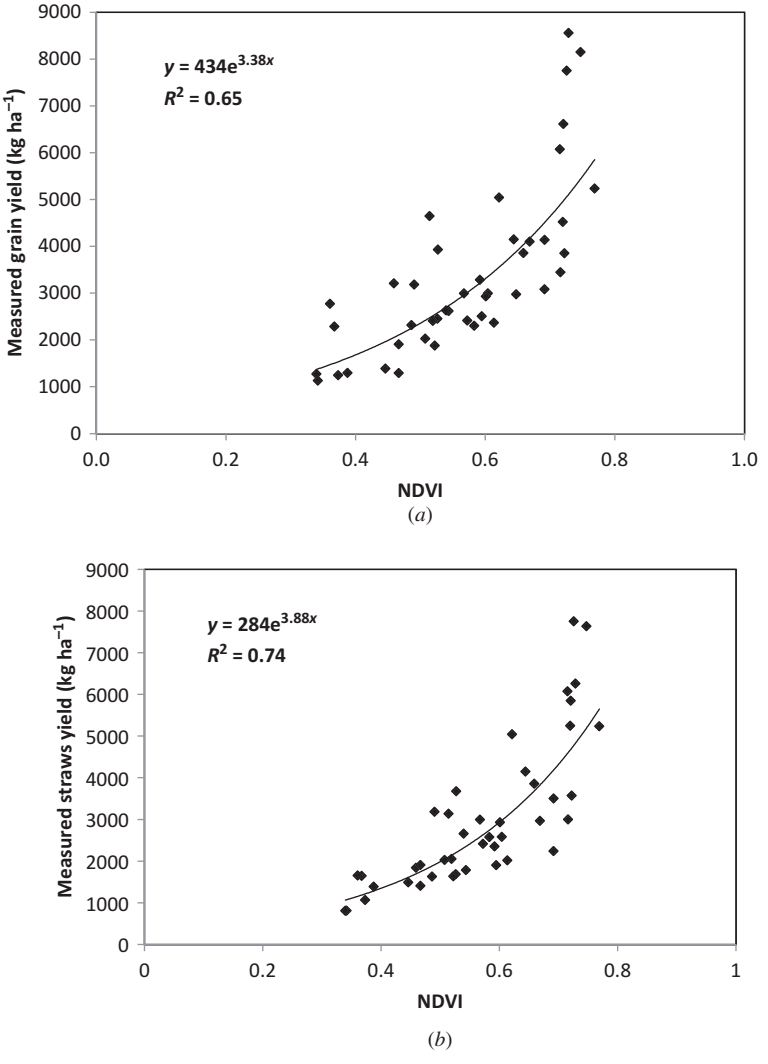

Figure 4. Relationship between mesured cereal yields (grain and straw) and the SPOT–NDVI index, on 17 March 2011 and 31 March 2012: (*a*) grain yields, (*b*) straw yields.

large range of sowing dates, as well as irrigation and fertilization schedules, two exponential relationships were determined empirically:

$$\begin{aligned} Y_{\text{grain}} &= 434\ \exp(3.38\text{NDVI}), \\ Y_{\text{straws}} &= 285\ \exp(3.88\text{NDVI}). \end{aligned} \tag{1}$$

NDVI is well correlated with the average weight of the harvested grain ($R^2 = 0.66$) and with the average weight of the straw ($R^2 = 0.74$). In the case of the data acquired before and after those corresponding to Figure 4, the correlation between the satellite index and the measured yields is weaker. In practice, the end of March corresponds to a maximum in vegetation dynamics. Before this date, NDVI variations between fields are not affected by

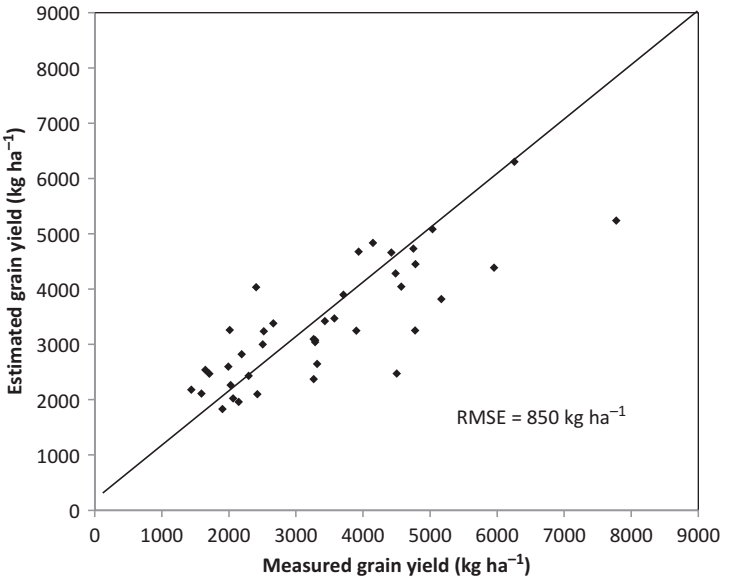

(*a*)

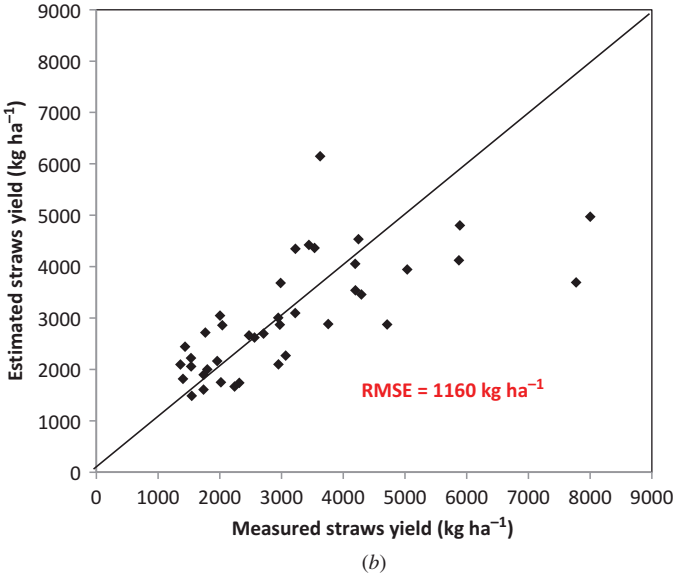

(*b*)

Figure 5. Comparison between measured and estimated cereal yields: (*a*) grain yields and (*b*) straw yields.

irrigation or rainfall events occurring in March, which are essential to grain development. In mid-April, the vegetation LAI starts to decrease, leading to a reduced capacity to distinguish between high and low grain yields.

Figure 5 plots the NDVI-estimated grain and straw yields as a function of the ground truth measurements, thus validating the proposed empirical algorithms for the second set of test fields: the resulting RMSE is equal to 850 kg ha^{-1} for grain yield and 1160 kg ha^{-1} for straw yield. This outcome demonstrates the robustness of the proposed empirical approach, despite its simplicity.

The same yield estimation algorithm was applied separately for the wheat and barley crops, independently of the various agricultural practices (sowing date, type of seeder, irrigation date, quantity of fertilizer, etc.). The results are described below.

3.1.1. Wheat yield

Figure 6 shows a plot of the exponential relationship between the measured yield (grain and straw) and NDVI for the first set of wheat fields tested. The measured yield and NDVI can be seen to be well correlated, with correlation coefficients R^2 equal to 0.67 and 0.66 for grain and straw, respectively.

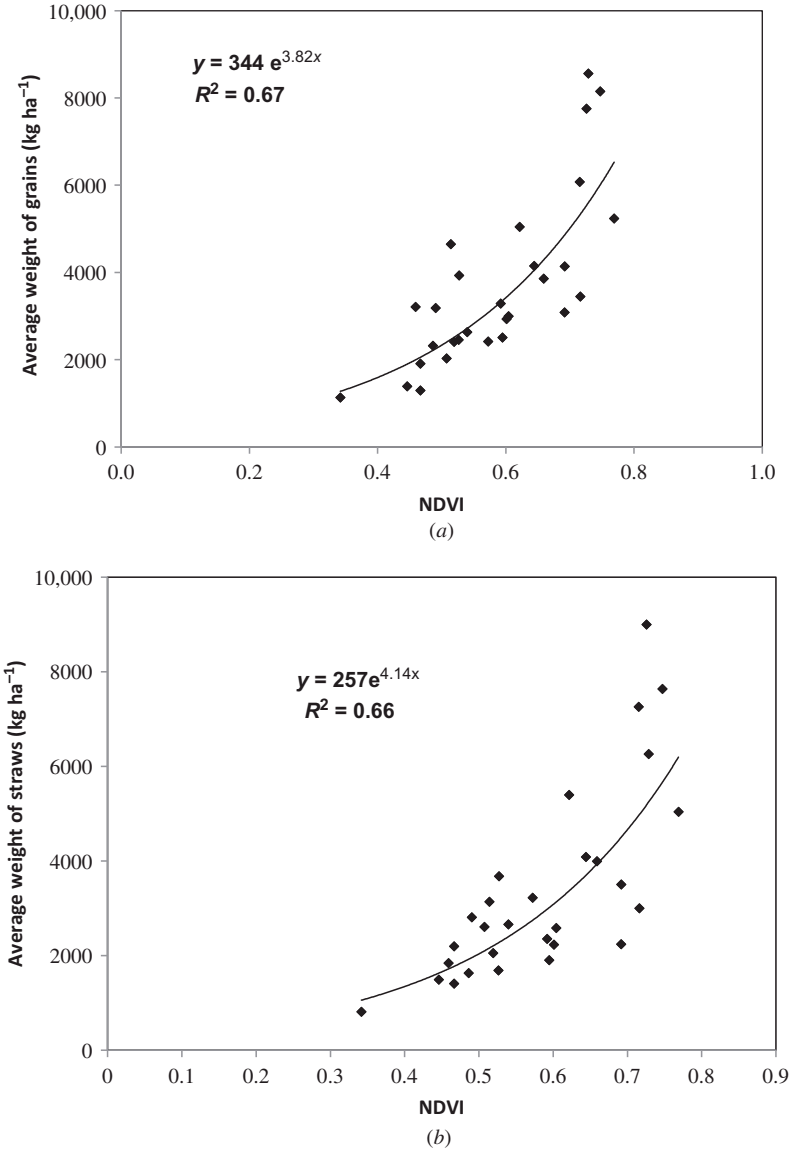

Figure 6. Relationship between measured wheat yields (grain (*a*) and straw (*b*)) and the SPOT-NDVI index on 17 March 2011 and 31 March 2012.

The empirical relationships were validated with a second set of test fields. The measured and estimated yields can be seen to be in good agreement, with an RMS error equal to 900 kg ha^{-1} and 1100 kg ha^{-1} for grain and straw, respectively (Figure 7).

3.1.2. Barley yield

Twenty-two barley fields were observed during the two agricultural years. The database was divided into two sets: the first was used to estimate the yield on the basis of the NDVI

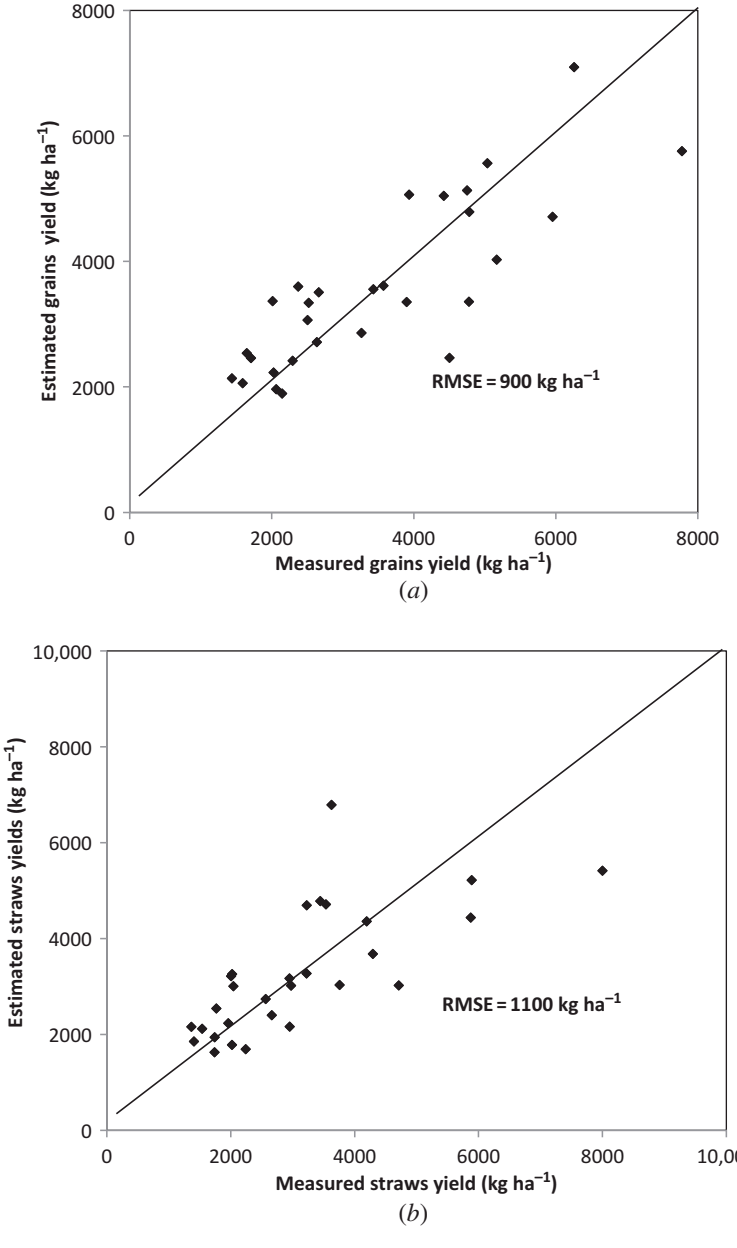

Figure 7. Comparison between measured and estimated wheat yields: (*a*) grain yields and (*b*) straw yields.

measurements, and the second set was used for model validation. Figure 8 provides a plot of the linear relationship established between measured and NDVI-derived grain and straw yields for the first set of test fields. The correlation coefficients R^2 are equal to 0.62 and 0.70 for grain and straw, respectively.

The proposed relationship was validated by comparing yield measurements and estimations with the second set of fields. The results are found to be in good agreement, with an RMS error equal to 650 kg ha^{-1} and 1470 kg ha^{-1} for grain and straw estimations,

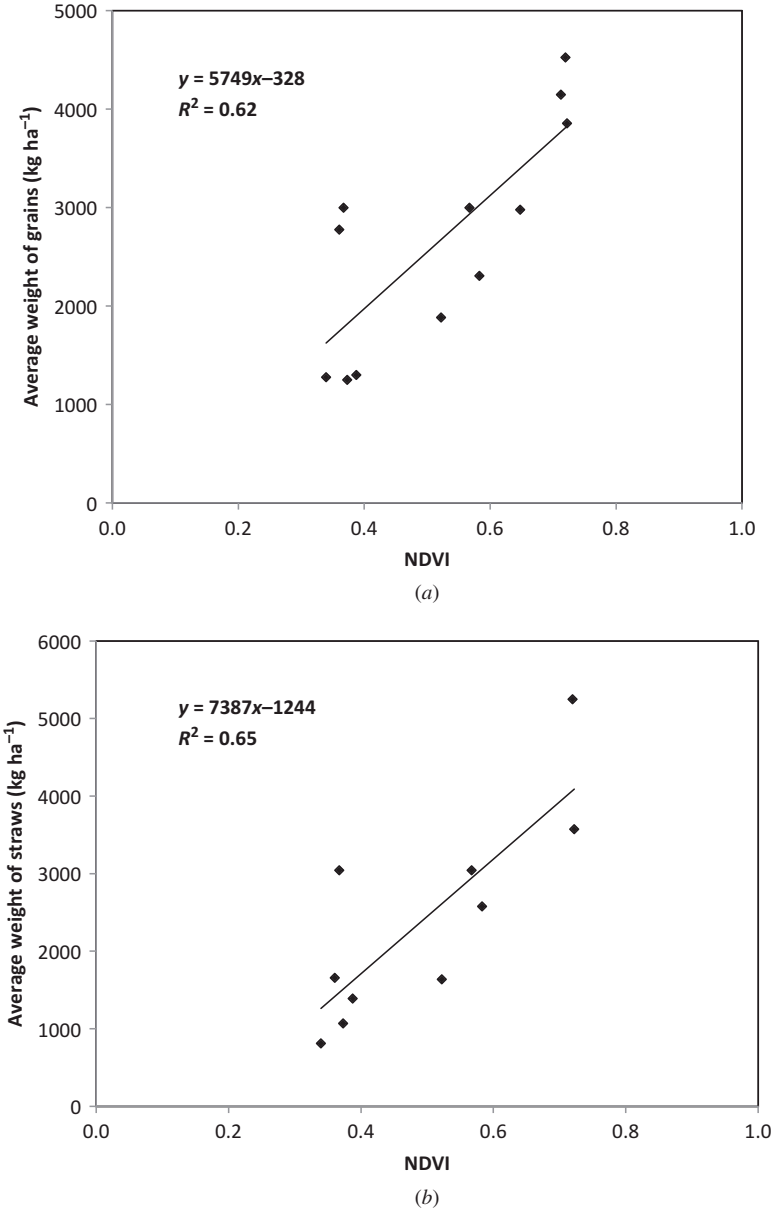

Figure 8. Relationship between measured barley yields (grain (*a*) and straw (*b*)) and the SPOT–NDVI index, on 17 March 2011 and 31 March 2012.

respectively (Figure 9). In the case of barley, only a linear relationship was considered, since the number of test fields was too small for a more complex (e.g. exponential) relationship to be determined.

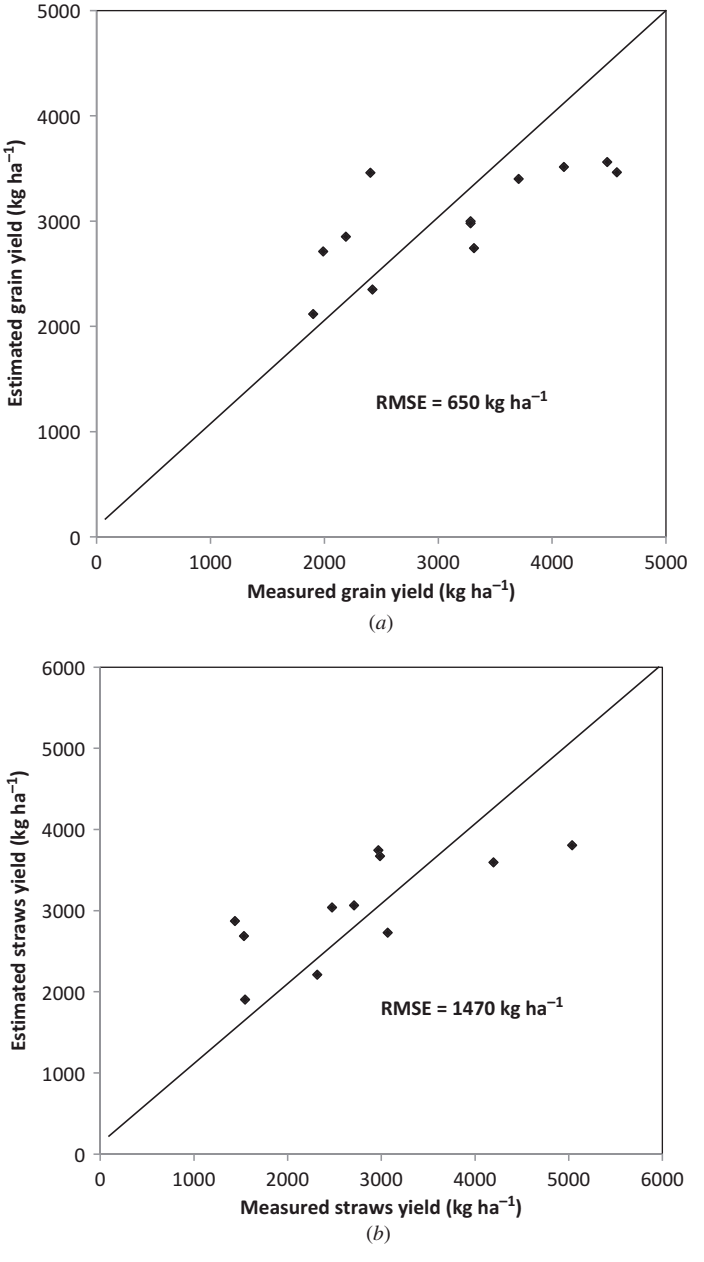

Figure 9. Comparison between measured and estimated barley yields: (*a*) grain yields and (*b*) straw yields.

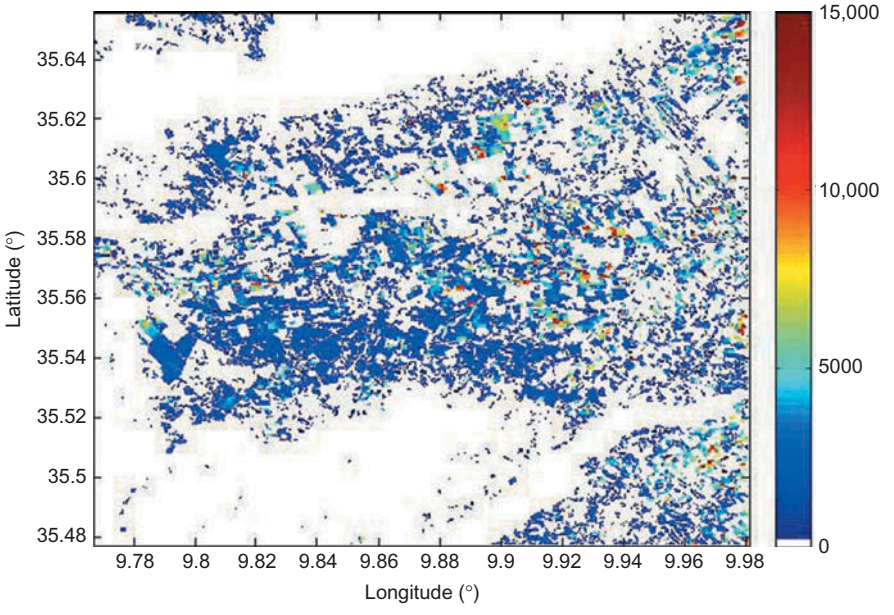

Figure 10. Cereal yield map for the 2011–2012 agricultural season.

3.2. *Yield mapping*

Following the above-described validation, Equation (1) was used to invert NDVI and generate yield maps for all classes of cereal. The wheat and barley classes could not be treated separately, because they were not differentiated by the land-use identification process.

In order to eliminate the influence of local terrain heterogeneities (due to local variations in vegetation cover and soil surface, etc.) on the processed optical signal, the yield was estimated over cells corresponding to 10 × 10 pixels (approximately 100 m^2), rather than at the scale of single pixels. For each resulting cell, the yield estimation was applied only if more than 25% of the cell's pixels belonged to cereal fields. The value of the computed yield could then be considered as representative of the entire cell. In Figure 10, the yield maps are shown for the 2011–2012 agricultural season.

4. Estimation of the dynamics and yields of cereals using the SAFY growth model

4.1. *SAFY model description*

One of the aims of the present study was to evaluate the potential use of time series of a variable biophysical parameter (the LAI) for the monitoring of phytomass production and the grain yield of cereal crops. This evaluation was based on the use of the SAFY model (Duchemin et al. 2008). The main idea was to use the model to represent well-known processes involved in crop development and growth, with the requirement that these processes be simulated using standard data, i.e. climatic data and optical imagery (which provides LAI estimations). Climatic data were generated by a weather station located in our study area (lat: 35.56°, long: 9.94°), which provided air temperature (T_a) and incoming global radiation (Rg) measurements. These data were recorded once every 30 min.

The model simulates the increase in dry above-ground phytomass, based on the light-use efficiency theory of Monteith (1977), and also takes the dynamics of green leaves and the influence of temperature into account (Duchemin et al. 2008). The dynamics of green LAI are simulated by estimating the extent of leaf coverage during growth (ΔLAI +) and the decrease in LAI during senescence due to the wilting and falling of leaves (ΔLAI–). These two phenological phases are identified through the use of a degree-day approach based on the accumulated air temperature (ΣT_a). Leaf senescence starts when ΣT_a has attained a given threshold S_{TT} (sum of temperature for senescence):

$$\begin{aligned} \Delta\mathrm{LAI}+ &= \Delta\mathrm{DAM} \times P_L(\Sigma T_a) \times \mathrm{SLA}, \\ \Delta\mathrm{LAI}- &= \mathrm{LAI}(\Sigma T_a - S_{TT})/R_s, \end{aligned} \tag{2}$$

where DAM is the dry, above-ground mass, P_L is the partition-to-leaf function (which can be expressed as an empirical function of the air temperature), SLA is the specific leaf area, and R_s is the rate of senescence.

SAFY has a low level of complexity in order to simplify the optimization of unknown parameters when a small number of observations is available. The parameters are limited in number (14), and are used to determine *a priori* values based on data provided by various prior experimental studies (Varlet-Grancher et al. 1982; Sinclair and Amir 1992; Meinke et al. 1998; Porter and Gawith 1999; Claverie et al. 2012). However, three of these parameters (the day of plant emergence (D_0), the effective light-use efficiency (ELUE), and the 'sum of temperature for senescence' (S_{TT}) are strongly dependent on the ambient agro-environmental conditions.

4.2. *Application of the SAFY model to cereal cycle retrieval*

The first step involves calibrating the three parameters (D_0, ELUE, S_{TT}). This procedure corresponds to the identification of an optimum parameter set from which, for each field, the SAFY simulation leads to the best reproduction of several observed variables. These parameters were calibrated using an optimization algorithm based on the observed ground truth LAI values collected in the fields. For each test plot, three optimized parameters were determined. These provided the 'best combination', defined as that having the lowest root mean square error (RMSE) between the LAI measured in the field and that estimated by the SAFY model. Table 4 indicates the range over which each of these parameters was considered.

The values of these three parameters are thus determined, for each test plot, on the basis of LAI measurements. The cereal dynamics are derived, for each field, from the estimated LAI. In Figure 11, the LAI determined with the model is compared to that measured on the ground, for four different fields planted with irrigated and rainfed cereals. It can be seen that in all four cases, the model accurately retrieves the dynamic range of the LAI. Maximum growth occurs at the end of March.

Table 4. Ranges over which the three optimized SAFY parameters are considered.

Parameter	Units	Range	Interval
$\boldsymbol{D_0}$	day	15–120	5
ELUE	g MJ^{-1}	0–10	0.2
$\boldsymbol{S_{TT}}$	°C	200–1800	10

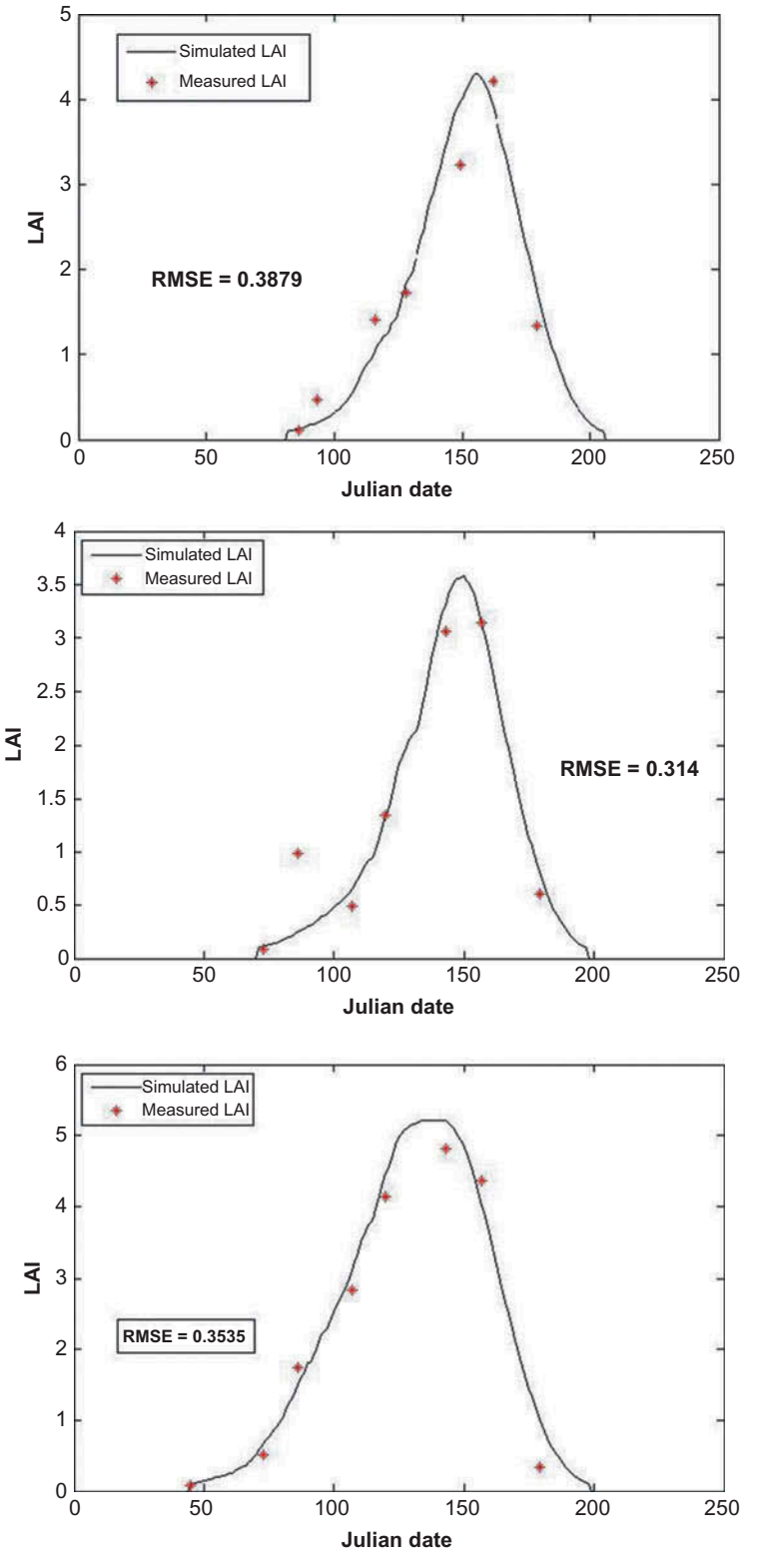

Figure 11. Green LAI dynamics for three different fields, estimated using the SAFY model, and ground measurements during the 2011–2012 agricultural season.

4.3. Application of the SAFY model to yield estimations

The grain-filling phase ranges from the day when foliage production ends to the day when total senescence occurs. During this period, the daily increase in grain yield (ΔGY) is proportional to the total above-ground phytomass (DAM), with a constant fraction P_y partitioned to grains, and thus:

$$\Delta GY = P_y \times DAM. \quad (3)$$

Since the characteristic parameters of the wheat and barley fields are quite different, the SAFY model was validated independently for each type of cereal. Field measurements were thus used to calibrate the fraction P_y, for each type of cereal, by minimizing the RMSE between the grain yields measured in all of the fields, and the wheat and barley grain yields simulated by the SAFY model ($P_{y\ wheat} = 0.0108$ and $P_{y\ barley} = 0.0057$).

Figure 12(*a*) compares the SAFY model yield estimations with ground measurements, in the case of barley fields. Although the ground measurements and model estimations are only moderately correlated ($R^2_{barley} = 0.35$), the SAFY model can be seen to produce results which are coherent with the ground measurements in terms of yield dynamics. The limitations of the SAFY model can be explained by various influences (fertilization, irrigation, etc.), which it does not take into account. In Figure 12(*b*), the SAFY model wheat yield estimations are compared to the ground measurements. As in the case of barley fields, only a moderate degree of correlation is found ($R^2_{wheat} = 0.33$) between the two types of data.

4.4. Application combining the SAFY model with remotely sensed data

In this section, multi-temporal satellite LAI measurements are used to calibrate the SAFY model. Before implementing this calibration, a relationship is established between the satellite NDVI and the LAI.

4.4.1. NDVI–LAI relationship for cereals

The LAI variable can be determined from NDVI. Several types of relationship can be found in the literature that compare these two key parameters. According to Wardley and Curran (1984), the NDVI-LAI relationship can be assumed to be linear, although when the LAI lies in the interval between 2 and 6 this relationship is no longer valid. Asrar et al. (1984) and Richardson et al. (1992) derived logarithmic relationships to express the NDVI as a function of LAI.

In the present study, for each pixel, a NDVI profile was generated from the satellite data. A relationship was then established between the NDVI and LAI of the studied test fields during the growing seasons of 2008–2009 and 2010–2011. As proposed by Duchemin et al. (2006), an exponential relationship of the following type was then determined:

$$NDVI = NDVI_\infty + (NDVI_{soil} - NDVI_\infty) \times e^{-k_{NDVI}\,LAI}, \quad (4)$$

where $NDVI_\infty$ is the asymptotic value of the NDVI derived from the measurements; in the case of the present study, $NDVI_\infty$ was taken to be 0.75 (see Figure 13(*a*)), and $NDVI_{soil}$ is the value of NDVI for bare soil (value determined in the present study: 0.15); k_{NDVI} is the extinction coefficient.

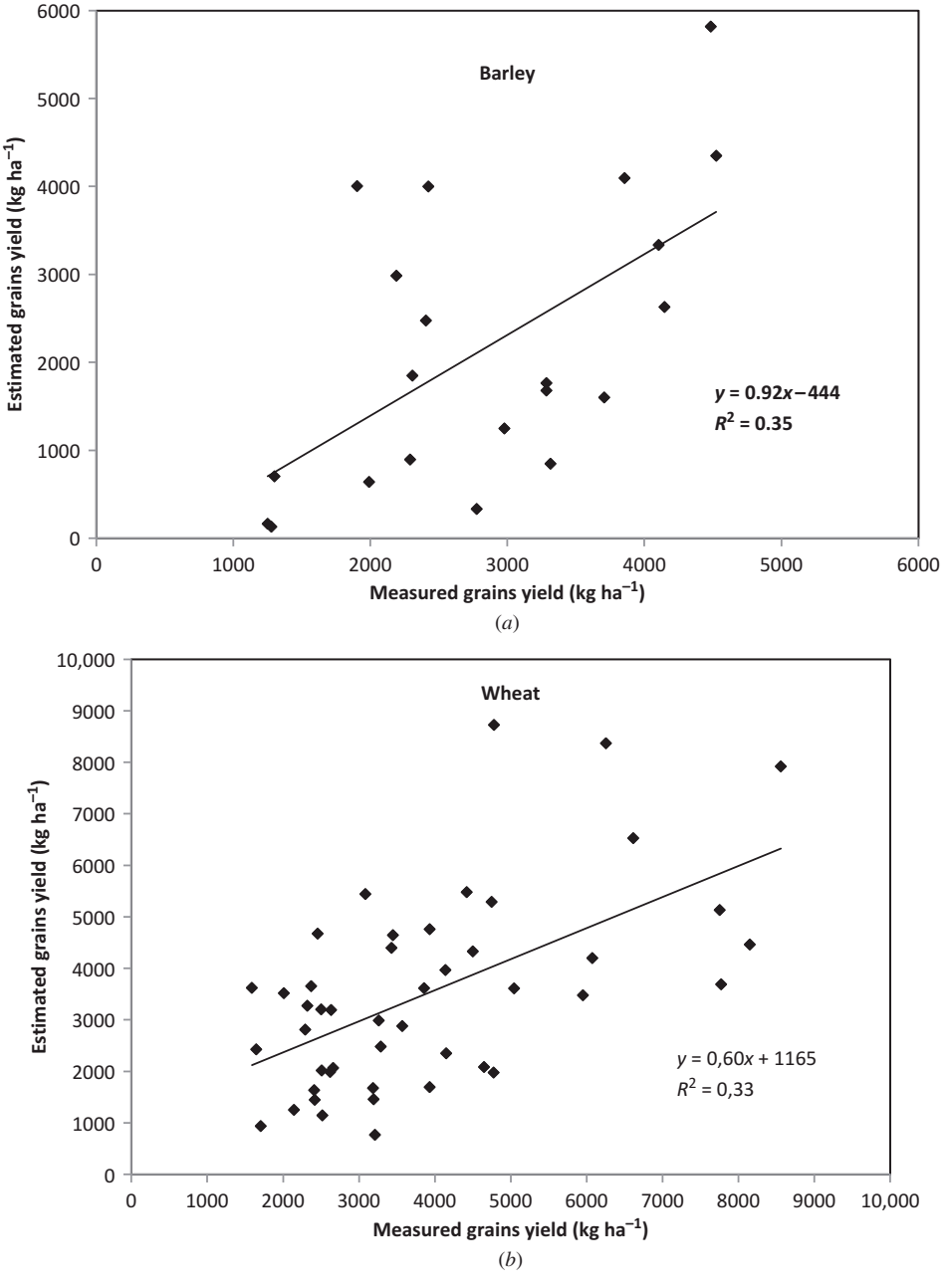

Figure 12. Comparisons between measured and estimated (SAFY model) grain yields, for barley (*a*) and wheat (*b*).

Figure 13(*a*) plots the experimental LAI–NDVI data points, corresponding to the 2009–2010 and 2011–2012 seasons, together with a least-squares fit to the above empirical relationship, which has a correlation coefficient of 0.78. It should be noted that when LAI exceeds 2, NDVI saturates (at approximately 0.75), leading to NDVI errors at high LAI values.

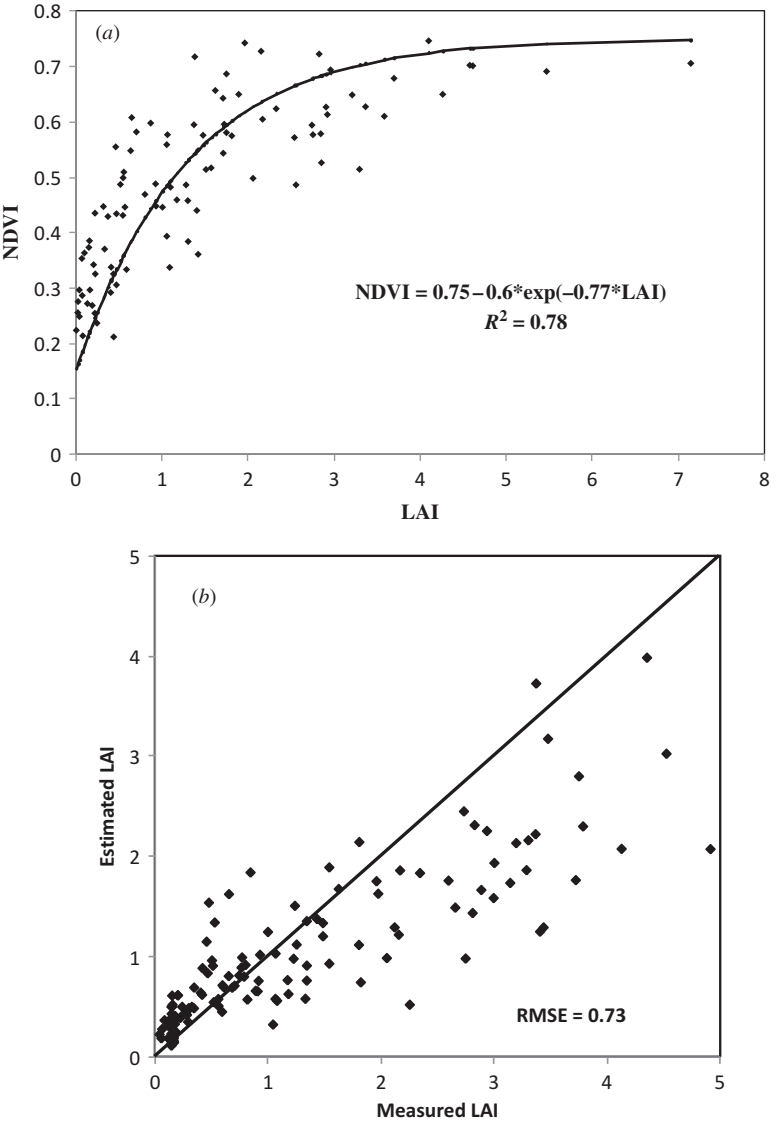

Figure 13. (*a*) Relationship between NDVI and LAI measured at the test fields. (*b*) Comparison between measured and estimated LAI using Equation (1), for the 2011–2012 agricultural season.

The proposed algorithm was validated by comparing ground truth measurements with estimations derived from SPOT NDVI data for the test fields.

The resulting RMSE is equal to 0.73, as shown in Figure 13(*b*). In accordance with the NDVI saturation effect noted above, the proposed empirical algorithm was found to be inaccurate for high LAI values.

4.4.2. Application of the SAFY model using satellite LAI estimations

In this section, the grain yield is estimated using the SAFY model combined with remotely sensed, multi-temporal SPOT acquisitions. This process involves initial

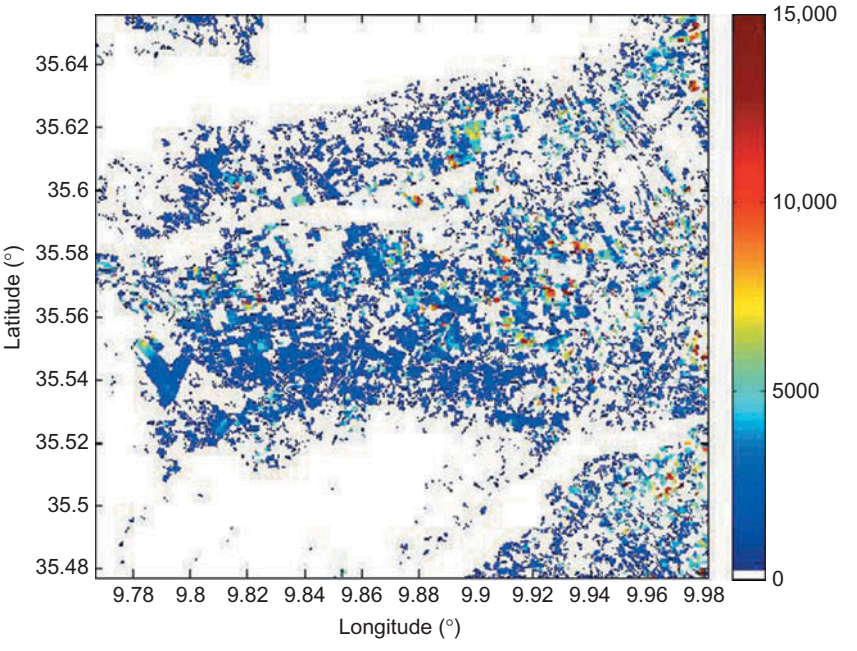

Figure 14. Cereal yield map produced by combining SPOT/HRV multi-temporal acquisitions and SAFY model data.

calibration of the SAFY model, achieved by minimizing the RMSE between the SPOT5-time series LAI and the SAFY model LAI. Maps of the three parameters – ELUE, D_0, and S_{TT} – optimized for the SAFY model, are thus generated. In order to eliminate the effects of local heterogeneities (due to irregularities occurring during the sowing and growth stages, vegetation dispersion heterogeneities, etc.), these three parameters are estimated over cells corresponding to 10 × 10 pixels (approximately 100 m^2). When more than 25% of each cell belongs to the relevant class of cereals, the estimated values of the three corresponding parameters are applied.

After having generating the (D_0, ELUE, S_{TT}) parameter maps, an empirical relationship $\Delta GY = P_y \times DAM + b$ was used to generate (wheat and barley) cereal yield maps. The SAFY model thus estimates grain yields over a 10 × 10 pixel window. The yield map corresponding to the 2011–2012 agricultural year is shown in Figure 14.

Figure 15(*a*) compares, for all pixels, the yield estimations computed using statistical remote sensing analysis (Section 3) with those determined by combining the SAFY model with remotely sensed measurements. In Figure 15(*b*), the difference between the two yield maps is shown for each pixel. The two estimations can be seen to be reasonably correlated, with R^2 equal to 0.45. Nevertheless, it should be noted that the SAFY model grain yields are underestimated. This could be explained by the fact that wheat and barley were not analysed separately in this study. It is possible that saturation of NDVI (at approximately 0.75), which leads to underestimated values of LAI, also contributes to an underestimation of the grain yields predicted by the SAFY model. In addition, the semi-empirical SAFY model has 14 input parameters, of which D_o, ELUE, and S_{TT} were calibrated in the present study. However, there are three crop-specific parameters (Pla, Plb, Rs), the values of which depend on the type of cereal (wheat or barley). Another limitation of the SAFY model is that it assumes ELUE to

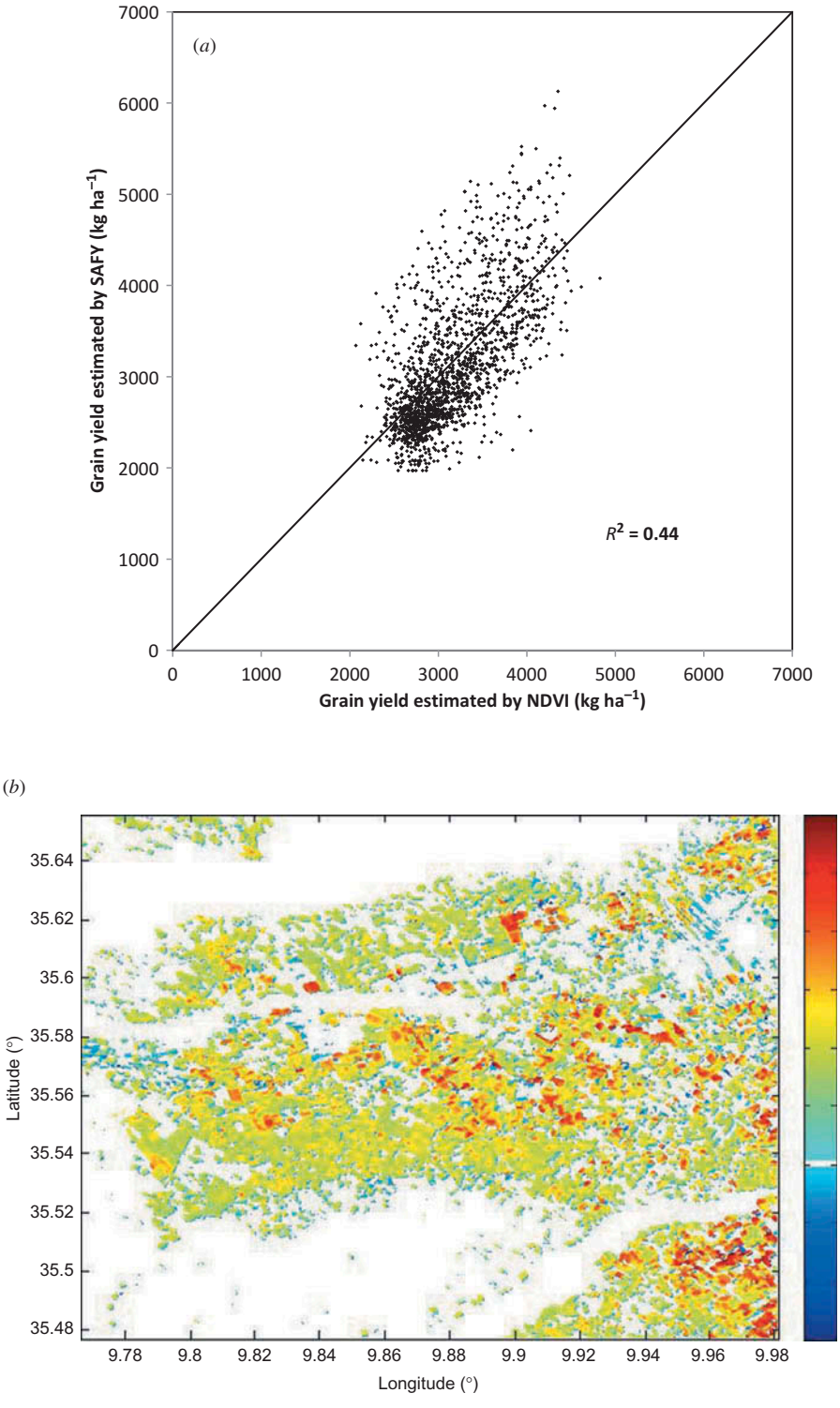

Figure 15. (*a*) Comparison between yield estimations computed using statistical remote-sensing analysis, and yields determined by combining remotely sensed data with the SAFY model. (*b*) Map showing the differences between the yields estimated from the NDVI and those computed with the SAFY model.

remain constant over each cereal's phenological cycle, whereas other studies show that ELUE decreases during the maturity phase (Lecoeur et al. 2011; Claverie et al. 2012).

5. Conclusion

The aim of this study was to characterize the dynamics and yields of various cereals in the semi-arid Merguellil catchment, using high-resolution optical data and a simple agro model.

In a first step, a statistical comparison between SPOT optical measurements and ground truth yields is proposed. The yield analysis for grain and straw as a function of NDVI reveals a strong correlation between these two variables, from mid-March to mid-April. An exponential relationship is retrieved between the yields and the remotely sensed NDVI index, with a correlation coefficient greater than 0.6. Validation of the remotely sensed estimations through the use of ground measurements shows that this approach is robust, with an RMS error equal to 850 and 1160 kg ha^{-1} for grain and straw yields, respectively. Exponential and linear relationships are determined for wheat and barley yields, based on the NDVI index. Validation of the proposed expressions leads to reasonable results, with an RMS error lower than 900 kg ha^{-1} for both types of cereal. On the basis of the aforementioned analysis and the validation process, yield maps are proposed for all classes of cereal at the study site.

In order to characterize the cereal cycle, a SAFY growth model is also used. This model provides excellent simulations of variations in the LAI for irrigated and rainfed cereal fields. In the case of the yield estimations, despite the limited accuracy (low correlation coefficient) of the model, coherent trends in the yield dynamics are retrieved for the study test fields. The tested model has the advantage of being relatively simple, without requiring the input of data related to agricultural practices (sowing, irrigation, and fertilization), and is thus very useful for operational applications on a regional scale.

Finally, the SAFY model is used in combination with remotely sensed LAI measurements. In an initial step, an exponential relationship is established between NDVI and LAI, both of which are derived from optical satellite data. An RMS error equal to 0.78 is found when these remotely sensed parameters are validated through the use of ground measurements. This relationship allows LAI to be mapped on cereal fields. Following calibration of the SAFY model through the use of multi-temporal LAI satellite maps, yield estimations are proposed for the entire study site. The maps produced from satellite measurements are found to be moderately well correlated with those determined by combining satellite measurements and SAFY model data (R^2 = 0.45). The cereal yields predicted by the SAFY model are found to underestimate the real values measured on the ground.

Acknowledgements

The authors extend their thanks to the officials of the Chebika Cereal Institute, the National Institute of Meteorology, and the Department of Soil and CRDA Kairouan, for their assistance during the test field measurements. The authors would also like to thank the technical team from the IRD (Institut de Recherche pour le Développement) and the INAT (Institut National Agronomique de Tunisie), for their collaboration in the acquisition of field data.

Funding

This study was funded by two programmes: the French SICMED/Mistrals programme and the French ANR's AMETHYST ANR-12-TMED-0006-01 project.

References

Amri, R., M. Zribi, B. Duchemin, Z. Lili-Chabaane, C. Gruhier, and A. Chebouni. 2011. "Analysis of Vegetation Behaviour in a Semi-Arid Region, Using SPOT-VEGETATION NDVI Data." *Remote Sensing* 3: 2568–2590.

Asrar, G., M. Fuchs, E. T. Kanemasu, and J. L. Hatfield. 1984. "Estimating Absorbed Photosynthetic Radiation and Leaf Area Index from Spectral Reflectance in Wheat." *Agronomy Journal* 76: 300–306.

Balaghi, R., B. Tychon, H. Eerens, and M. Jlibene. 2008. "Empirical Regression Models Using NDVI, Rainfall and Temperature Data for the Early Prediction of Wheat Grain Yields in Morocco." *International Journal of Applied Earth Observation and Geoinformation* 10: 438–452.

Baret, F., B. De Solan, R. Lopez-Lozano, K. Ma, and M. Weiss. 2010. "GAI Estimates of Row Crops from Downward Looking Digital Photos Taken Perpendicular to Rows at 57.5 Degrees Zenith Angle: Theoretical Considerations Based on 3d Architecture Models and Application to Wheat Crops." *Agricultural and Forest Meteorology* 150: 1393–1401.

Barnett, T. L., and D. R. Thompson. 1982. "The Use of Large-Area Spectral Data in Wheat Yield Estimation." *Remote Sensing of Environment* 12: 509–518.

Bastiaanssen, W. G. M., and S. Ali. 2003. "A New Crop Yield Forecasting Model Based on Satellite Measurements Applied Across the Indus Basin, Pakistan." *Agriculture, Ecosystems and Environment* 94: 321–340.

Bastiaanssen, W. G. M., M. Menenti, R. A. Feddes, and A. A. M. Holtslag. 1998. "A Remote Sensing Surface Energy Balance Algorithm for Land (SEBAL). 1. Formulation." *Journal of Hydrology* 212–213: 198–212.

Becker-Reshef, I., E. Vermote, M. Lindeman, and C. Justice. 2010. "A Generalized Regression-Based Model for Forecasting Winter Wheat Yields in Kansas and Ukraine Using MODIS Data." *Remote Sensing of Environment* 114: 1312–1323.

Benedetti, R., and P. Rossinni. 1993. "On the Use of NDVI Profiles as a Tool for Agricultural Statistics: The Case Study of Wheat Yield Estimate and Forecast in Emilia Romagna." *Remote Sensing of Environment* 45: 311–326.

Berthelot, B., and G. Dedieu. 1997. "Correction of Atmospheric Effects for VEGETATION Data." In *Physical Measurements and Signatures in Remote Sensing,* edited by G. Guyot and T. Phulpin, 19–25. Courchevel: Balkema.

Claverie, M., V. Demarez, B. Duchemin, O. Hagolle, D. Ducrot, C. Marais-Sicre, J. F. Dejoux, M. Huc, P. Keravec, P. Béziat, R. Fieuzal, E. Ceschia, and G. Dedieu. 2012. "Maize and Sunflower Biomass Estimation in Southwest France Using High Spatial and Temporal Resolution Remote Sensing Data." *Remote Sensing of Environment* 124: 844–857.

Deblonde, G., and J. Cihlar. 1993. "A Multiyear Analysis of the Relationship Between Surface Environmental Variables and NDVI Over the Canadian Landmass." *Remote Sensing Reviews* 7: 151–177.

Duchemin, B., R. Hadria, S. Erraki, G. Boulet, P. Maisongrande, A. Chehbouni, R. Escadafal, J. Ezzahar, J. C. B. Hoedjes, M. H. Kharrou, S. Khabba, B. Mougenot, A. Olioso, J. C. Rodriguez, and V. Simmonneaux. 2006. "Monitoring Wheat Phenology and Irrigation in Central Morocco: On the Use of Relationships Between Evapotranspiration, Crop Coefficients, Leaf Area Index and Remotely-Sensed Vegetation Indices." *Agricultural Water Management* 79: 1–27.

Duchemin, B., P. Maisongrande, G. Boulet, and I. Benhadj. 2008. "A Simple Algorithm for Yield Estimates: Evaluation for Semi-Arid Irrigated Winter Wheat Monitored with Green Leaf Area Index." *Environmental Modelling & Software* 23: 876–892.

Field, C. B., J. T. Randerson, and C. M. Malmstrom. 1995. "Global Net Primary Production: Combining Ecology and Remote Sensing." *Remote Sensing Environment* 51: 74–88.

Justice, C. O., and I. Becker-Reshef. 2007. *Report from the Workshop on Developing a Strategy for Global Agricultural Monitoring in the Framework of Group on Earth Observations (GEO),* 1−67. College Park: Geography Department, University of Maryland.

Kirk, K., H. J. Andersen, A. G. Thomsen, J. R. Jørgensen, and R. N. Jørgensen. 2009. "Estimation of Leaf Area Index in Cereal Crops Using Red–Green Images." *Biosystems Engineering* 104: 308–317.

Kogan, F., N. Kussul, T. Adamenko, S. Skakun, O. Kravchenko, O. Kryvobok, A. Shelestov, A. Kolotii, O. Kussul, and A. Lavrenyuk. 2013. "Winter Wheat Yield Forecasting in Ukraine Based on Earth Observation, Meteorological Data and Biophysical Models." *International Journal of Applied Earth Observation and Geoinformation* 23: 192–203.

Laurila, H., M. Karjalainen, J. Kleemola, and J. Hyyppa. 2010. "Cereal Yield Modeling in Finland Using Optical and Radar Remote Sensing." *Remote Sensing* 2: 2185–2239.
Lecoeur, J., R. Poire-Lassus, A. Christophe, B. Pallas, P. Casadebaig, P. Debaeke, F. Vear, and L. Guilioni. 2011. "Quantifying Physiological Determinants of Genetic Variation for Yield Potential in Sunflower. SUNFLO: A Model-Based Analysis." *Functional Plant Biology* 38: 246–259.
Lobell, D. B., G. P. Asner, J. I. Ortiz-Monasterio, and T. L. Benning. 2003. "Remote Sensing of Regional Crop Production in the Yaqui Valley, Mexico: Estimates and Uncertainties." *Agriculture, Ecosystems and Environment* 94: 205–220.
Maselli, F., M. Chiesi, L. Brilli, and M. Moriondo. 2012. "Simulation of Olive Fruit Yield in Tuscany Through the Integration of Remote Sensing and Ground Data." *Ecological Modelling* 244: 1–12.
Meinke, H., G. L. Hammer, H. van Keulen, and R. Rabbinge. 1998. "Improving Wheat Simulation Capabilities in Australia From a Cropping Systems Perspective III. The Integrated Wheat Model (I_WHEAT)." *European Journal of Agronomy* 8: 101–116.
Meygret, A. 2005. *Absolute Calibration: From SPOT1 to SPOT5.* San Diego, CA: SPIE.
Monteith, J. L. 1972. "Solar Radiation and Productivity in Tropical Ecosystems." *Journal of Applied Ecology* 9: 747–766.
Monteith, J. L. 1977. "Climate and the Efficiency of Crop Production in Britain." *Philosphical Transaction of the Royal Society of London Series B* 281: 277–294.
Moriondo, M., F. Maselli, and M. Bindi. 2007. "A Simple Model of Regional Wheat Yield Based on NDVI Data." *European Journal of Agronomy* 26: 266–274.
Porter, J. R., and M. Gawith. 1999. "Temperatures and the Growth and Development of Wheat: A Review." *European Journal of Agronomy* 10: 23–36.
Prasad, A. K., L. Cha, R. P. Sing, and M. Kafatos. 2006. "Crop Yield Estimation Model for Iowa Using Remote Sensing and Surface Parameters." *International Journal of Applied Earth Observation and Geoinformation* 8: 26–33.
Propastin, P., and M. Kappas. 2009. "Modeling Net Ecosystem Exchange for Grassland in Central Kazakhstan by Combining Remote Sensing and Field Data." *Remote Sensing* 1: 159–183.
Rahman, H., and G. Dedieu. 1994. "SMAC: A Simplified Method for the Atmospheric Correction of Satellite Measurements in the Solar Spectrum." *International Journal of Remote Sensing* 15: 123–143.
Richardson, A. J., C. L. Wiegand, D. F. Wanjura, D. Dusek, and J. L. Steiner. 1992. "Multisite Analyses of Spectral Biophysical Data for Sorghum." *Remote Sensing of Environment* 41: 71–82.
Rouse, J. W., R. H. Haas, J. A. Schell, and D. W. Deering. 1974. "Monitoring the Vernal Advancement and Retrogradation (Green Wave Effect) of Natural Vegetation." In *Progress Report RSC 1978–1*. College Station, TX: Remote Sensing Center, Texas A&M University.
Sandmann, M., J. Graefe, and C. Feller. 2013. "Optical Methods for the Non-Destructive Estimation of Leaf Area Index in Kohlrabi and Lettuce." *Scientia Horticulturae* 156: 113–120.
Sellers, P. J. 1985. "Canopy Reflectance, Photosynthesis and Transpiration." *International Journal Remote Sensing* 6: 1335–1372.
Sinclair, T. R., and J. Amir. 1992. "A Model to Assess Nitrogen Limitations on the Growth and Yield of Spring Wheat." *Field Crops Research* 30: 63–78.
Varlet-Grancher, C., R. Bonhomme, M. Chartier, and P. Artis. 1982. "Efficience De La Conversion De L'e´Nergie Solaire Par Un Couvert Végétal." *Acta Oecologia/Oecologia Plantarum* 17: 3–26.
Wang, Y. P., K. W. Chang, R. K. Chen, J. C. Lo, and Y. Shen. 2010. "Large-Area Rice Yield Forecasting Using Satellite Imageries." *International Journal of Applied Earth Observation and Geoinformation* 12: 27–35.
Wardley, N. W., and P. J. Curran. 1984. "The Estimation of Green Leaf Area Index from Remotely Sensed Airborne Multispectral Scanner Data." *International Journal of Remote Sensing* 4: 671–679.
Wei-guo, L., L. Hua, and Z. Li-Hua. 2011. "Estimating Rice Yield by HJ-1a Satellite Images." *Rice Science* 18 (2): 142–147.
Ye, X., K. Sakai, L. O. Garciano, S. I. Asada, and A. Sasao. 2006. "Estimation of Citrus Yield from Airborne Hyperspectral Images Using a Neural Network Model." *Ecological Modeling* 198: 426–432.
Zribi, M., C. André, and B. Decharme. 2008. "A Method for Soil Moisture Estimation in Western Africa Based on ERS Scatter Meter." *IEEE Transactions on Geoscience and Remote Sensing* 46 (2): 438–448.
Zribi, M., A. Chahbi, M. Shabou, Z. Lili-Chabaane, B. Duchemin, N. Baghdadi, R. Amri, and G. Chehbouni. 2011. "Soil Surface Moisture Estimation Over a Semi-Arid Region Using ENVISAT ASAR Radar Data for Soil Evaporation Evaluation." *Hydrology Earth System Sciences* 15: 345–358.